

Differential Current Decay Profiles of Epithelial Sodium Channel Subunit Combinations in Polarized Renal Epithelial Cells*

Received for publication, May 7, 2004, and in revised form, May 25, 2004
Published, JBC Papers in Press, May 27, 2004, DOI 10.1074/jbc.M405091200

Savita Mohan, Jennifer R. Bruns, Kelly M. Weixel‡, Robert S. Edinger, James B. Bruns, Thomas R. Kleyman, John P. Johnson, and Ora A. Weisz§

From the Laboratory of Epithelial Cell Biology, Renal-Electrolyte Division, Department of Medicine, University of Pittsburgh, Pittsburgh, Pennsylvania 15261

In many epithelial tissues in the body, the rate of Na^+ reabsorption is governed by the activity of the epithelial sodium channel (ENaC). The assembly, trafficking, and turnover of the three ENaC subunits (α , β , and γ) is complex and not well understood. Recent experiments suggest that ENaC must be proteolytically cleaved for maximal activity and may explain the discrepancies reported in prior biochemical approaches focused on quantitating the trafficking and half-life of full-length subunits. As an alternative approach to examining the dynamics of ENaC subunits, we have generated doxycycline-repressible replication-defective recombinant adenoviruses encoding individual epitope-tagged mouse ENaC subunits and expressed these in polarized MDCK I cells. Co-infection with these viruses encoding all three subunits generates robust amiloride-sensitive currents in polarized MDCK cells. Significant current was also observed in cells expressing α - and γ -mENaC in the absence of β -mENaC. These currents did not appear to result from association with endogenous canine β -ENaC. Treatment of $\alpha\beta\gamma$ -expressing cells with cycloheximide (CHX) resulted in the rapid inhibition (within 3 h) of ~50–80% of the initial current; however, a sizable fraction of the initial current remained even after 6 h of CHX. By contrast, CHX addition to cells expressing only α - and γ -mENaC resulted in rapid decay in current with no residual fraction. Our data suggest that ENaC channels of differing stoichiometries are differentially trafficked and degraded and provide support for the possibility that noncoordinate trafficking of ENaC subunits may function *in vivo* as a mechanism to modulate ENaC activity.

rate-limiting step in sodium reabsorption in a number of tissues (reviewed in Ref. 1). Given the clinical importance of ENaC activity, the assembly, trafficking, and response to hormonal stimulation of ENaC subunits have been subjects of considerable study and debate. While biochemical studies from several laboratories universally report a short half-life for the total pool of newly synthesized ENaC subunits (typically 1–2 h) (2–7), there is considerable dispute regarding the stability of ENaC subunits that have reached the plasma membrane. Some studies report rapid decay of all three cell surface subunits in polarized MDCK and A6 cells (4, 5), whereas we and others have observed long half-lives of α - and γ -ENaC that were biotinylated at the apical plasma membrane of A6 cells (6, 8). We use the term noncoordinate regulation to describe this differential turnover of ENaC subunits and have proposed possible molecular models for this observation based on experimental results from many laboratories (6, 9).

Considerable data suggest that activation of ENaC channels is regulated by proteolytic enzymes (10–12). Recently, new evidence has emerged that suggests that activation of ENaC involves direct furin-mediated cleavage of α - and γ -ENaC subunits within the biosynthetic pathway (13, 14). These results suggest that changes in biochemical levels of full-length ENaC subunits may not correlate directly with modulation of sodium currents.

Because sodium current rather than biochemical levels of ENaC subunits is the ultimate expression of ENaC activity, we have taken an alternative approach to examining ENaC trafficking and dynamics by measuring the stability of ENaC current upon inhibition of new protein synthesis. To do this, we generated replication-defective recombinant adenoviruses (AVs) encoding epitope-tagged α -, β -, and γ -mENaC and used these to infect polarized MDCK I cells. Whereas uninfected cells have very low endogenous ENaC activity, co-infection of MDCK I cells with AVs encoding all three ENaC subunits generates a robust amiloride-sensitive, sodium-dependent current. Moreover, protein expression in our system is dependent on transcription via the tetracycline operon and can therefore be reversibly inhibited by inclusion of low levels of doxycycline in the growth medium. This system therefore offers tremendous flexibility in our ability to regulate the expression of ENaC subunits in a renal epithelial cell line that maintains physiologic regulatory mechanisms. Using this system, we have observed distinct current decay profiles in cycloheximide (CHX)-treated cells infected with different combinations of ENaC subunits. Our results suggest that stoichiometry-dependent trafficking of ENaC subunit combinations could serve as a physiologic mechanism to regulate sodium reabsorption *in vivo*.

The epithelial sodium channel (ENaC)¹ is an apical heterotetramer containing α , β , and γ subunits that serves as the

* This work was supported by National Institutes of Health (NIH) R01 Grants DK57718 (to J. P. J. and O. A. W.) and DK65161 (to T. R. K.) and by an individual National Research Service Award (to S. M.). The laboratory of epithelial cell biology is supported in part by funds from Dialysis Clinic, Inc. The costs of publication of this article were defrayed in part by the payment of page charges. This article must therefore be hereby marked "advertisement" in accordance with 18 U.S.C. Section 1734 solely to indicate this fact.

‡ Supported by NIH Grant T32-DK61296.

§ To whom correspondence should be addressed: Renal-Electrolyte Division, University of Pittsburgh, 3550 Terrace St., Pittsburgh, PA 15261. Tel.: 412-383-8891; Fax: 412-383-8956; E-mail: weisz@pitt.edu.

¹ The abbreviations used are: ENaC, epithelial sodium channel; AV, adenovirus; CHX, cycloheximide; DOX, doxycycline; I_{sc} , short circuit current; MDCK, Madin-Darby canine kidney; m.o.i., multiplicity of infection; mENaC, mouse ENaC; xENaC, *Xenopus* ENaC; RT, reverse transcriptase; PBS, phosphate-buffered saline.

MATERIALS AND METHODS

Cell Lines and Adenoviruses—MDCK type I cells were maintained in Dulbecco's modified Eagle's medium/F-12 (Invitrogen) supplemented with 10% fetal bovine serum, streptomycin (100 $\mu\text{g/ml}$) and penicillin (100 units/ml). The generation of cDNAs for mouse ENaC (mENaC) subunits epitope-tagged on their carboxyl termini (V5 tag on α - and γ -mENaC; FLAG tag on β -mENaC) is described in Ref. 13. The constructs were amplified by PCR and subcloned downstream of the tetracycline operon in the pAdtet vector using HindIII and SpeI restriction sites. Full-length β - and γ -xENaC were provided by Dr. Douglas Eaton and subcloned into pAdtet using standard cloning techniques. Replication-defective recombinant AVs were generated using the method described in Ref. 15. Unless otherwise stated, cells were seeded at high density ($\sim 2 \times 10^5$ cells/well) on 12-mm transwells (0.4- μm pore; Costar, Cambridge, MA) for 3–5 days prior to infection with recombinant AV at a multiplicity of infection (m.o.i.) of 60 for each subunit unless otherwise indicated. For optimal infection, filter-grown cells were rinsed extensively with calcium-free PBS containing 1 mM MgCl_2 (PBS- Mg^{2+}). Subsequently, individual transwells were incubated for 1 h at 37 °C on 50- μl drops of PBS- Mg^{2+} -containing virus, with an additional 150 μl of PBS- Mg^{2+} /virus placed on the apical surface of the transwell. Samples were then returned to normal growth medium. Recombinant adenovirus (m.o.i. 60–100) encoding the constitutive expression of tetracycline-repressible transactivator was included in all experiments to enable doxycycline-repressible synthesis of ENaC subunits. Experiments were initiated the day after infection.

PCR Analysis and Partial Cloning of Canine β -ENaC—Total RNA was isolated from 2×75 -mm transwells of MDCK I cells using the RNAqueous kit (Ambion). Single-stranded cDNA was generated from 1 μg of total RNA using the ProtoScript kit (New England Biolabs). The cDNA was amplified by PCR using primers designed against ENaC subunit nucleotide sequences that are invariant between *Xenopus*, rat, mouse, and human ENaC: α (5'-CTTCTGCAACAA(C/T)ACCACCA-TCC; 3'-GATGGAGGTCTCCAC(C/T)CCAGGC); β (5'-(G/T)T(A/G)AC(-A/T)GAGTGGTACATCTGTC; 3'-AAT(A/T)CCCTTCTGCTCAGG-TG); and γ (5'-AA(C/T)ATCATGGCACAGGTGCCTC; 3'-AGCATCTCA-ATACTGTTGGCTG). PCR products were cloned into pTOPO-BluntII (Invitrogen). Clones containing PCR products were sequenced. To obtain the C-terminal sequence of canine β -ENaC, a new 5'-specific primer (AACACATGATCCAGAAGTGC) and a degenerate 3' primer (CTAGATGGCCTCCACCTC(A/G)CTTGTC) against the 3'-untranslated region were generated. PCR and analysis were performed as above.

Antibodies and Indirect Immunofluorescence—Monoclonal anti-V5 antibody was purchased from Invitrogen. Although our β -mENaC construct is tagged with the FLAG epitope, we found that antibodies directed against β -ENaC were more effective at detecting this construct than commercially available anti-FLAG antibodies. The characterization of polyclonal antibodies directed against the carboxyl-terminal sequence of β -xENaC is described in Ref. 16. This antibody recognizes β -mENaC in methanol-fixed cells and efficiently immunoprecipitates β -mENaC. An additional anti- β -ENaC antibody directed against the tail sequence of rat/mouse β -ENaC was the kind gift of Dr. Mark Knepper (17). To localize α - and γ -mENaC-expressing cells, virally infected filter-grown MDCK I cells were rinsed with PBS, fixed for 20 min with 3% paraformaldehyde at ambient temperature, and then quenched briefly with PBS containing 10 mM glycine and 0.02% sodium azide (PBS-G) and permeabilized for 3 min in PBS-G containing 0.5% (v/v) Triton X-100. To localize cells expressing β -mENaC, cells were fixed with -20 °C methanol for 10 min. The subsequent steps were similar for both fixation conditions. After blocking nonspecific binding sites with 0.25% ovalbumin in PBS-G, filters were incubated with primary antibody (mouse monoclonal anti-V5 (1:200 dilution) or affinity-purified rabbit polyclonal anti- β -xENaC (1:100 dilution)) for 20 min. The filters were then washed extensively and incubated with Cy3 or Cy2 conjugated with goat anti-mouse or goat anti-rabbit antibodies respectively (Jackson ImmunoResearch Laboratories) as appropriate. After further washing, filters were cut from their inserts, mounted onto glass slides, and viewed at $\times 60$ magnification using a Nikon EFD-3 microscope. Images were captured using a Hamamatsu C5985 cooled CCD camera and processed using Adobe Photoshop software (Adobe Systems Inc.).

Radiolabeling and Immunoprecipitation—Virally infected MDCK cells were starved in cysteine- and methionine-free medium, radiolabeled using Tran³⁵S-label (50 $\mu\text{Ci/ml}$; MP Biomedicals) for 1 h and chased in serum-free modified Eagle's medium. At the appropriate chase time, cells were rinsed with PBS and lysed in detergent solu-

tion (6). After a brief centrifugation to remove nuclei, lysates were immunoprecipitated with anti- β -ENaC or -V5 antibodies, and antibody-antigen complexes were collected using fixed *Staphylococcus aureus* (Pansorbin; Calbiochem) or protein G-coupled Sepharose (Sigma), respectively. After washing with radioimmune precipitation buffer (10 mM Tris-HCl, pH 7.4, 0.15 M NaCl, 1% Triton X-100, 1% deoxycholate, 1% Nonidet P-40, 0.1% SDS), samples were electrophoresed on 10% SDS-PAGE gels and analyzed using a Personal FX phosphorimager (Bio-Rad).

Electrophysiological Measurement of Current Decay in Cycloheximide-treated Cells—A $100\times$ concentrated stock of cycloheximide (10 mg/ml; Sigma; prepared in MDCK I medium) was added to both the apical and basolateral surfaces of the transwell without changing the medium, and the cells were returned to the incubator. MDCK I cells treated with this concentration of CHX maintained normal transepithelial resistances for at least 7 h. Equivalent short circuit currents (I_{sc}) were measured in a sterile hood at the indicated time intervals using an electrode voltage ohmmeter from World Precision Instruments. The electrode was calibrated using growth medium prior to measurement of the potential difference and resistance across the filter. Resistance was normalized to the surface area of the transwell. Current was calculated using the potential difference across the filter divided by the resistance normalized to surface area to obtain readings measured in $\mu\text{A}/\text{cm}^2$. The rate of current decay was analyzed using OriginPro 6.1 statistical software (OriginLab). Data were fit to exponential decay functions; the statistically best fit for each data set was obtained with first order exponential decay fit to the equation $y = y_0 + A_1 e^{-x/t_1}$. Fit of the data was not improved by use of two exponential functions or linear functions. For analysis of current decay in both $\alpha\beta\gamma$ - and $\alpha\gamma$ -expressing cells, $R^2 > 0.97$ for all fits to first order exponential decay.

RESULTS

Adenovirus-mediated Expression of mENaC Subunits in MDCK I Cells—Our studies utilized high resistance type I MDCK cells, which have been used previously for studies on the trafficking of heterologously expressed ENaC subunits (4, 7). When grown as polarized monolayers on filter supports, we measured a very low I_{sc} ($0.27 \pm 0.02 \mu\text{A}/\text{cm}^2$; $n = 12$) that was unaffected by the addition of 100 μM amiloride. Stimulation by overnight treatment with aldosterone or brief treatment with vasopressin increased currents to $0.87 \pm 0.13 \mu\text{A}/\text{cm}^2$ ($n = 3$) and $0.85 \pm 0.13 \mu\text{A}/\text{cm}^2$ ($n = 3$), respectively, but did not affect the amiloride-sensitive component.²

To determine whether AV infection provides an effective method to express functional ENaC channels in these cells, we infected filter-grown polarized monolayers with recombinant AVs encoding epitope-tagged α -, β -, and/or γ -mENaC subunits. An AV encoding constitutively expressed tetracycline transactivator, required to drive expression from the tetracycline operon, was also included. Both α - and γ -mENaC carry C-terminal V5 tags, whereas β -mENaC is tagged with the FLAG epitope. The following day, cells were starved, metabolically labeled for 1 h, and solubilized, and ENaC subunits were immunoprecipitated using anti-V5 (Fig. 1A). Both α - and γ -mENaC subunits were readily detected in cells expressing either individual subunits or all three subunits. Similarly, antibodies directed against either mouse or *Xenopus* β -ENaC tail peptides efficiently precipitated AV-expressed β -mENaC (Fig. 1B).

To confirm that AV infection of these MDCK cells is efficient, we performed indirect immunofluorescence on filter-grown MDCK I cells infected with AVs encoding all three mENaC subunits (Fig. 1C). α - and γ -mENaC were co-visualized using monoclonal anti-V5 antibody, whereas β -mENaC was visualized using a polyclonal antibody raised against β -xENaC. Whereas the fixation requirements for these antibodies precluded double-labeling, we routinely observed bright staining in $>60\%$ of cells in each field. By contrast, no staining was detected in mock-infected cells.

² S. Mohan, J. R. Bruns, and O. A. Weisz, unpublished observations.

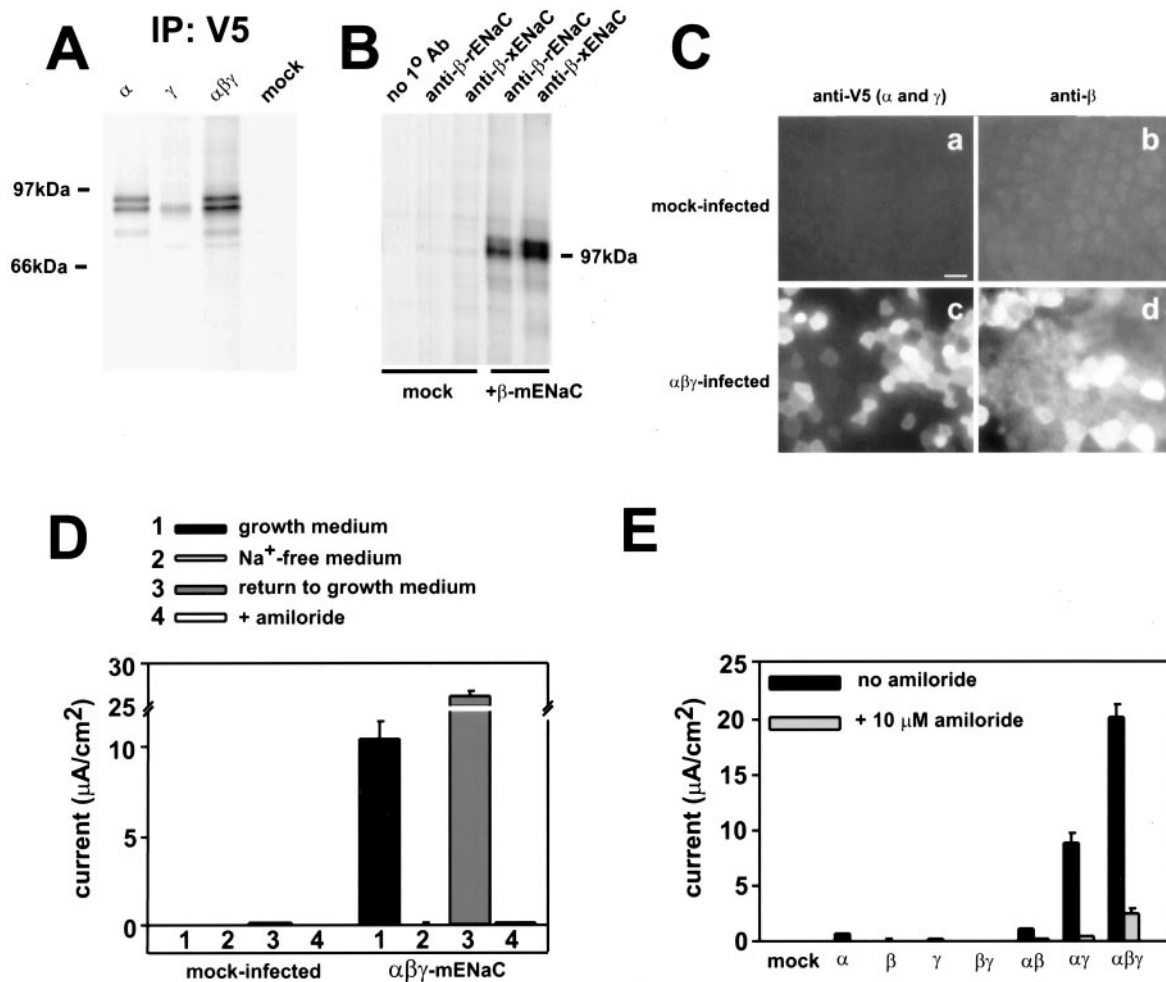


FIG. 1. AV-mediated expression of mENaC subunits in MDCK I cells generates sodium-dependent, amiloride-sensitive current. *A*, MDCK cells were mock-infected or co-infected with AVs encoding the tetracycline transactivator and the indicated combinations of mENaC subunits. The following day, cells were starved in methionine-free medium for 30 min, radiolabeled for 1 h, and solubilized. α - and γ -mENaC were immunoprecipitated using anti-V5 antibody. Samples were electrophoresed on 10% SDS-PAGE gels and examined using a phosphorimager. The migration of molecular weight standards is shown. *B*, MDCK I cells (mock-infected or infected with AV encoding β -mENaC) were starved, radiolabeled for 1 h, and then solubilized and immunoprecipitated with polyclonal antibodies directed against rat/mouse or *Xenopus* β -ENaC sequences. No primary antibody was included in a mock-infected sample as a control. *C*, polarized MDCK I cells were mock-infected (*a* and *b*) or infected with AVs encoding α -, β -, and γ -mENaC (*c* and *d*). The following day, cells were fixed and processed for indirect immunofluorescence with anti-V5 antibody (to detect α - and γ -subunits; *a* and *c*) or anti- β antibody (*b* and *d*). *D*, infection with AVs encoding α -, β -, and γ -mENaC generates sodium-dependent, amiloride-sensitive current in MDCK I cells. Current was monitored in mock-infected cells and cells infected with AVs encoding α -, β -, and γ -mENaC incubated first in standard growth medium and then shifted to sodium-free medium and returned to standard medium and then after the addition of 100 μM amiloride. *E*, infection with combinations of mENaC subunits generates amiloride-sensitive current in MDCK I cells. MDCK I cells were mock-infected or infected with AVs encoding ENaC subunits individually or in combinations as shown. The following day, currents were measured before and after the addition of 10 μM amiloride.

Quantitation of short circuit currents in polarized MDCK I cells infected with AVs encoding all three ENaC subunits revealed sizable currents (Fig. 1*D*). I_{sc} was completely blocked when sodium in the medium was replaced by *N*-methyl-D-glucamine and recovered when sodium was restored. Moreover, the majority of current was inhibited when 100 μM amiloride was added. We generally measured an increase in I_{sc} upon the addition of fresh growth medium to ENaC-expressing MDCK I cells, and this could account for the overshoot in amiloride-sensitive I_{sc} that we observed upon replacement of sodium-free medium with normal growth medium.

We then examined the ability of ENaC subunits expressed in varying combinations to generate amiloride-sensitive I_{sc} in polarized MDCK cells. Expression of individual ENaC subunits or of $\alpha\beta$ or $\beta\gamma$ alone did not produce significant currents in these cells (Fig. 1*E*). However, coexpression of α - and γ -mENaC typically yielded amiloride-sensitive currents that were ~30–40% of those observed in cells infected with AVs encoding all three subunits. This is somewhat higher than previous reports,

which have suggested that expression of α - and γ -ENaC in *Xenopus* oocytes generates up to ~20% of maximal I_{sc} (18).

Current Decay in mENaC-expressing MDCK Cells Treated with CHX—To examine the stability of ENaC current at the cell surface in the absence of new protein synthesis, we monitored the effect of CHX on I_{sc} in polarized MDCK I cells infected with AVs encoding all three ENaC subunits or α - and γ -mENaC (Fig. 2). Control experiments demonstrated that this concentration of CHX (100 $\mu\text{g}/\text{ml}$) very rapidly decreased the rate of protein synthesis to 0.03% of control.² The decay in I_{sc} in $\alpha\gamma$ -expressing cells was rapid and essentially complete by 8 h of CHX treatment. By contrast, the addition of CHX to $\alpha\beta\gamma$ -expressing cells resulted in an initially rapid decline in I_{sc} that leveled off after 2–3 h and remained relatively stable for the remainder of the incubation. Table I shows the half-time of decay calculated from five independent experiments performed using identical expression conditions for $\alpha\beta\gamma$ - and $\alpha\gamma$ -expressing cells. The pattern of initial current decay was best fit by a single exponential decay function with a mean time constant of

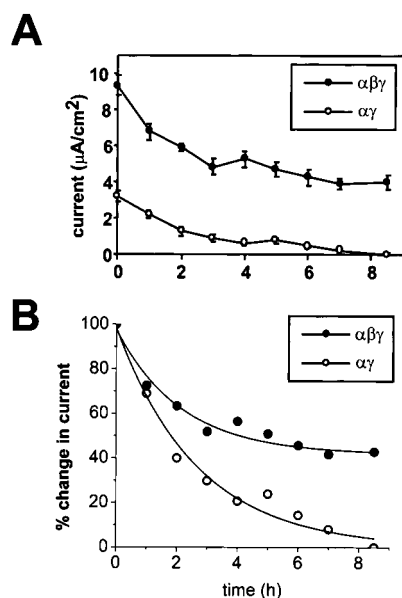


FIG. 2. Current decay of mENaC subunit combinations in cytoheximide-treated MDCK I cells. A, MDCK I cells infected with AVs encoding α - and γ -mENaC or all three subunits were incubated with 100 $\mu\text{g/ml}$ CHX, and equivalent short circuit current was monitored over an 8.5-h period. The mean \pm range of duplicate samples is plotted. A, raw data; B, the same data plotted with initial currents normalized to 100% and fit to a single exponential decay curve (see “Materials and Methods”; $R^2 = 0.97$ for $\alpha\beta\gamma$; $R^2 = 0.98$ for $\alpha\gamma$).

TABLE I
Time constants and residual currents in $\alpha\beta\gamma$ - versus $\alpha\gamma$ -expressing MDCK I cells

The initial rate of current decay in $\alpha\beta\gamma$ - and $\alpha\gamma$ -expressing MDCK I cells was fit to a single exponential decay curve and used to extrapolate the half-time of decay. Residual current was calculated as the fraction of initial current remaining 6 h after the addition of CHX. The results from five independent experiments performed using identical AV infection conditions are shown. The raw data from Experiment 4 are plotted in Fig. 3A. The mean time constants of decay measured for $\alpha\beta\gamma$ - versus $\alpha\gamma$ -expressing cells were not statistically different from one another, whereas residual currents were significantly different ($p < 0.001$ by Student’s t -test).

Experiment	Time constant		Residual I_{sc} at 6 h	
	$\alpha\beta\gamma$	$\alpha\gamma$	$\alpha\beta\gamma$	$\alpha\gamma$
	h		% $t = 0$	
1	2.01	1.87	43.5	7.0
2	3.72	2.51	29.8	11.1
3	2.87	1.56	31.8	7.0
4	2.13	2.66	45.7	14.4
5	2.04	2.01	43.4	7.4

2.56 h \pm 0.74 for $\alpha\beta\gamma$ -expressing cells and 2.12 h \pm 0.46 for $\alpha\gamma$ -expressing cells ($n = 5$; mean \pm S.D.). An example of the curve fitting is shown in Fig 2B. It is readily apparent that whereas all of the current decayed exponentially in $\alpha\gamma$ -expressing cells, the fit curve accounts for the decay of only $\sim 50\%$ of the initial current in $\alpha\beta\gamma$ -expressing cells. The addition of amiloride after long CHX treatments reduced the current to that measured in uninfected MDCK I cells (not shown). These data are consistent with the possibility that cells infected with α - and γ -mENaC express a single population of channels, whereas $\alpha\beta\gamma$ -expressing cells may assemble channels of multiple stoichiometries with distinct current decay profiles (e.g. $\alpha\gamma$ and $\alpha\beta\gamma$). Alternatively, the current decay profile we observed for $\alpha\beta\gamma$ -expressing cells may reflect two distinct populations of $\alpha\beta\gamma$ channels: a rapidly decaying pool that turns over with kinetics similar to the channels in $\alpha\gamma$ -expressing cells and a residual long lived pool.

The Current Decay Profile Is Independent of ENaC Expres-

sion Level—To determine whether the difference in current decay profile between $\alpha\beta\gamma$ - and $\alpha\gamma$ -expressing cells was related to the higher initial currents we typically observed in $\alpha\beta\gamma$ -expressing cells, we compared current decay profiles from multiple experiments with a range of initial currents. To maximize the overlap between $\alpha\beta\gamma$ and $\alpha\gamma$ starting currents, we limited our analysis to experiments in which the initial currents in $\alpha\beta\gamma$ -expressing cells were below 20 $\mu\text{A/cm}^2$. Fig. 3A shows the raw current traces measured upon CHX addition to $\alpha\gamma$ -expressing cells (black lines) versus $\alpha\beta\gamma$ -expressing cells (gray lines). Normalization of the initial I_{sc} in each trace to 100% (Fig. 3B) demonstrates that the difference between $\alpha\beta\gamma$ and $\alpha\gamma$ current decay profiles is independent of initial I_{sc} . On average, we found that $45.1 \pm 2.3\%$ of initial I_{sc} remained after 3 h of CHX treatment, and $30.9 \pm 2.5\%$ of base-line I_{sc} remained after 6 h in $\alpha\beta\gamma$ -expressing cells ($n = 13$; mean \pm S.E.). By contrast, currents dropped to $26.3 \pm 2.4\%$ and $9.3 \pm 1.5\%$ of the initial values in cells expressing only α - and γ -mENaC after 3 and 6 h of CHX treatment, respectively ($n = 5$).

The variability in I_{sc} that we observed between experiments could reflect differences in ENaC expression per cell or, alternatively, differences in AV infection efficiency. Therefore, to confirm that the current decay profile upon CHX addition was independent of cellular ENaC expression level, we used doxycycline (DOX) to regulate the amount of ENaC expressed in cells after viral infection. Cells were co-infected with AVs encoding all three subunits, and DOX (0.03 ng/ml) was added to some samples immediately upon removal of the AV. This treatment resulted in a marked decrease in the I_{sc} measured the following day (Fig. 3C, $t = 0$). However, upon the addition of CHX, both the rate of current decay and the fraction of residual I_{sc} remaining after 6 h of CHX treatment were similar in DOX-treated versus untreated cells (Fig. 3D). Thus, it is unlikely that the residual I_{sc} reflects saturation of the cellular capacity to internalize or degrade ENaC.

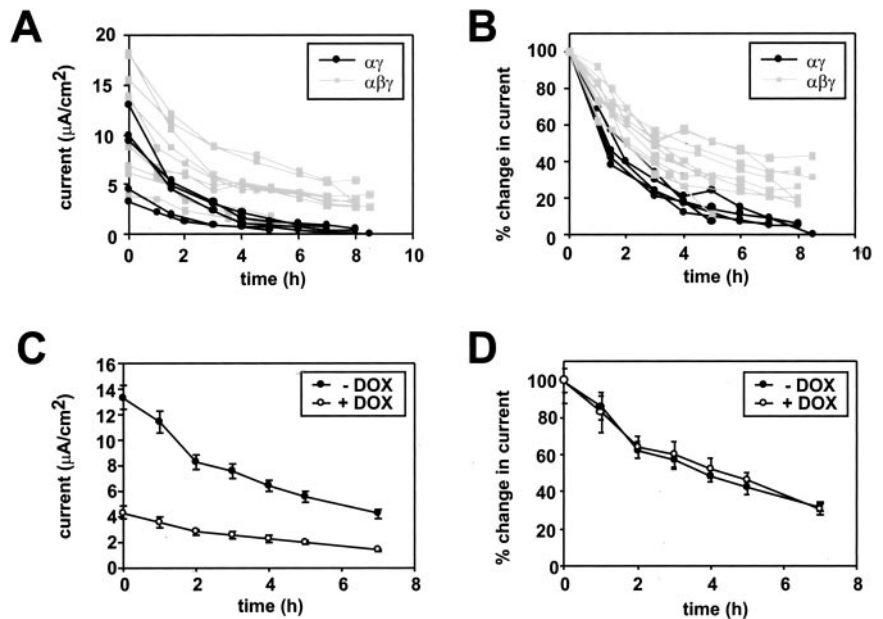
MDCK I Cells Express Undetectable Levels of Endogenous β -ENaC Subunit—We next considered the possibility that the I_{sc} we observed in MDCK I cells infected with AVs encoding α - and γ -mENaC was due to assembly of these subunits with endogenous canine β -ENaC. Species-specific trafficking motifs in the canine β -ENaC sequence might then account for the distinct decay curves we obtained in cells expressing only α - and γ -mENaC. To examine whether endogenous ENaC mRNA is expressed in our MDCK I cells, we first employed RT-PCR using conserved ENaC primers designed against highly conserved nucleotide sequences in each subunit to amplify total RNA isolated from polarized MDCK I cells (Fig. 4A). Whereas we obtained a significant signal when RNA was amplified using β -ENaC-specific primers, only trace levels of α - and γ -ENaC RNA were detected.

Based on the sequence of the amplified PCR product, a new 5'-specific primer and a degenerate 3' primer against the 3'-untranslated region of β -ENaC were generated and used to amplify the carboxyl-terminal sequence of canine β -ENaC. Repeated attempts to clone the amino-terminal region were unsuccessful. The carboxyl-terminal amino acid sequences of canine ENaC and mENaC were highly homologous and did not differ within regions thought to be important in regulating ENaC trafficking or stability (Fig. 4B).

We then examined whether endogenous β -ENaC protein could be immunoprecipitated from polarized MDCK I cells. Alignment of canine and rat/mouse β -ENaC sequences revealed only two amino acid differences within the region used to raise anti-peptide antibodies against rat/mouse ENaC (Fig. 4C). In addition, we used an antibody directed against a peptide from the C-terminal region of *Xenopus* β -ENaC to immu-

FIG. 3. ENaC current decay profiles are independent of expression level.

A, raw data from multiple experiments in which current decay was monitored after CHX addition to MDCK I cells expressing α - and γ -mENaC (black lines) or all three mENaC subunits ($\alpha\beta\gamma$; gray lines). **B**, the same traces with the initial currents at the time of CHX addition normalized to 100%. **C**, MDCK cells were infected with AVs encoding all three ENaC subunits and incubated overnight with or without 0.03 ng/ml DOX. The following day, I_{sc} decay was monitored after the addition of CHX. **D**, the initial currents at the time of CHX addition were normalized to 100%. Similar results were observed in two independent experiments where the initial I_{sc} was varied by severalfold by the addition of DOX.



noprecipitate radiolabeled MDCK I cells. Canine and mouse β -ENaC are identical to one another within the peptide sequence used to generate the anti-xENaC antibody (Fig. 4C). However, whereas both anti-mouse and anti-*Xenopus* β -ENaC antibody readily immunoprecipitated AV-expressed β -mENaC, they failed to detect endogenous protein (Fig. 1B). Moreover, we could not detect endogenous β -ENaC in MDCK I cells upon immunoprecipitation with anti-*Xenopus* β -ENaC and subsequent Western blotting using the anti-rat/mouse β -ENaC antibody (Fig. 4D). A background band of ~ 105 kDa was routinely observed; however, treatment of MDCK I immunoprecipitates with *N*-glycanase prior to gel electrophoresis and Western blotting revealed only a minor shift in the mobility of this band, inconsistent with the six potential *N*-glycosylation sites in our partial canine β -ENaC sequence. A band of similar molecular weight has previously been detected in MDCK cell lysates and dog kidney samples blotted using the same antibody (19). We also observed a similar background band in MDCK lysates immunoprecipitated with and then blotted using anti- β -xENaC.³ By contrast, AV-expressed β -mENaC was readily detected in MDCK cell lysates, and the mobility of this protein was markedly shifted by *N*-glycanase treatment. Finally, we examined whether a pool of endogenous β -ENaC might be stabilized upon infection with AVs encoding α - and γ -mENaC; however, no canine β -ENaC was detected in these cells (Fig. 4D). We conclude that whereas MDCK I cells express ENaC subunit mRNA, they have undetectable levels of ENaC subunit protein and channel activity.

The Current Decay Profile of $\alpha\beta\gamma$ -ENaC Is Species-independent—We next considered whether the C-terminal epitope tags on β - (or γ -) mENaC might contribute to the residual current we observed in $\alpha\beta\gamma$ -mENaC-expressing cells. To test this, we co-infected MDCK I cells with AVs encoding α -mENaC and non-epitope-tagged β - and γ -xENaC. This combination of ENaC subunits typically generated currents comparable with those we observed in $\alpha\beta\gamma$ mENaC-expressing cells. The current decay profile upon the addition of CHX to these cells was similar to that typically observed in cells expressing only mENaC subunits, with roughly 60% of the initial current remaining at 3 h (Fig. 5A). By contrast, CHX addition to $\alpha\gamma$ -

mENaC-expressing cells in the same experiment resulted in much a more rapid decay in I_{sc} ($\sim 70\%$ decay in 3 h).

Residual Current Correlates with β -mENaC Expression—Our data suggest that MDCK I cells expressing all three subunits contain at least two populations of ENaC channels: a rapidly decaying pool and a stable pool. One hypothesis is that the initial rapid current decay upon CHX treatment to $\alpha\beta\gamma$ -expressing cells represents the efficient turnover of a population of $\alpha\gamma$ channels in these cells, whereas the stable, residual current reflects the slow turnover of cell surface $\alpha\beta\gamma$ channels. Alternatively, all channels in $\alpha\beta\gamma$ -expressing cells may have the same stoichiometry, but a subpopulation may be resistant to turnover. A prediction of the first hypothesis is that increasing the relative amount of β -mENaC expression relative to α - and γ -mENaC might drive the assembly of $\alpha\beta\gamma$ channels, resulting in an increased fraction of residual I_{sc} upon CHX treatment. To test this, we infected MDCK I cells with AVs encoding α - and γ -mENaC at an m.o.i. of 60 each as usual and varied the amount of AV encoding β -mENaC from an m.o.i. of 0–60. I_{sc} in cells expressing no β -mENaC (Fig. 6, $\alpha\gamma$) declined rapidly as expected with essentially no residual current after 6 h. The addition of AV- β -mENaC at an m.o.i. of 20 or 60 resulted in a progressive increase in both the initial I_{sc} and in the fraction remaining after long CHX treatment. These results are consistent with a model in which ENaC subunits can be assembled into multiple stoichiometries that are differentially turned over after reaching the plasma membrane.

DISCUSSION

We have examined the stability of ENaC current upon inhibition of new protein synthesis in MDCK I cells. Whereas the majority of initial current in cells expressing all three subunits decayed quite rapidly over a 4-h period, a sizable fraction of the original amiloride-sensitive current remained stable over long time periods (up to 8.5 h). Similar results were observed over a wide range of initial currents, suggesting that the residual current does not reflect saturation of a trafficking or degradation pathway. By contrast, current in cells expressing only α - and γ -mENaC decayed rapidly, with little or no residual current remaining after several hours of CHX treatment. The difference between current decay profiles in $\alpha\gamma$ - versus $\alpha\beta\gamma$ -expressing cells was independent of initial current and does not appear to be due to α - and γ -mENaC assembly with endoge-

³ J. R. Bruns and O. A. Weisz, unpublished observations.

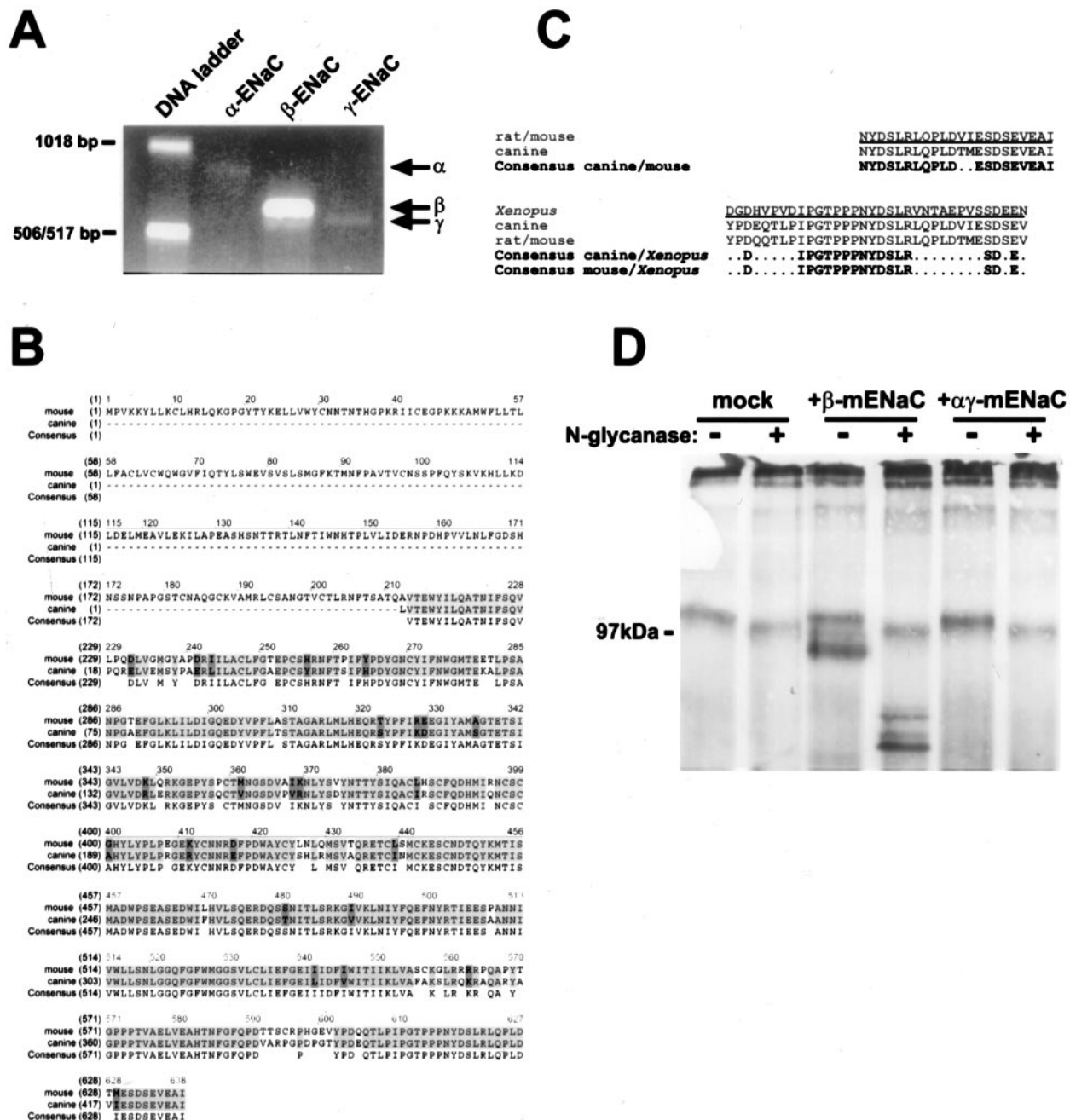


FIG. 4. Characterization of endogenous ENaC subunit expression in MDCK I cells. *A*, expression of endogenous ENaC mRNA in MDCK I cells. RNA isolated from polarized MDCK I cells was amplified by RT-PCR using universal primers complementary to invariant nucleotide sequences found in *Xenopus*, mouse, rat, and human α , β , or γ -ENaC. The expected sizes of PCR products based on mENaC sequences are 955, 672, and 803 bp for α , β , and γ subunits, respectively. Bands consistent with the expected sizes of α - and β -ENaC and a slightly smaller than expected band for γ -ENaC were observed (arrows), with β -ENaC present in greatest abundance. *B*, the partial sequence of canine β -ENaC obtained by RT-PCR amplification of RNA isolated from polarized MDCK I cells. *C*, homology between mouse/rat, canine, and *Xenopus* β -ENaC within the regions used to raise anti-peptide antibodies. *Upper panel*, the sequence against which the anti-mouse/rat antibody was raised is *underlined* and shown in *gray*, with the corresponding sequence of canine- β -ENaC directly below. The consensus within this region is shown in *black*. *Lower panel*, The sequence against which the anti-*Xenopus* antibody was raised is *underlined* and shown in *gray*, along with the corresponding sequences of canine and mouse β -ENaC. The consensus between either canine or mouse and *Xenopus* β -ENaC is identical and is shown in *black*. *D*, polarized MDCK cells (mock-infected or infected with AVs encoding the indicated subunits) were immunoprecipitated using a polyclonal antibody raised against β -xENaC and treated or mock-treated with *N*-glycanase. After electrophoresis, samples were Western blotted using a polyclonal antibody raised against the carboxyl-terminal sequence of rat/mouse β -ENaC as shown in *C*.

nous canine β -ENaC. Our data suggest the existence of at least two populations of ENaC channels in cells expressing all three subunits: a rapidly decaying pool and a stable pool.

MDCK type I cells have several characteristics that make them an ideal cell line for these studies. These cells grow as polarized monolayers with high transepithelial resistance, are amenable to infection with replication-defective recombinant

AVs, and have low endogenous current that is insensitive to amiloride. Although we detected β -ENaC mRNA in filter-grown cells, the cells do not express detectable levels of this subunit as determined by Western blotting or by immunoprecipitation of radiolabeled cells using two anti- β -ENaC peptide antibodies. Infection of these cells with AVs proved a useful means to generate high levels of amiloride-sensitive current. In

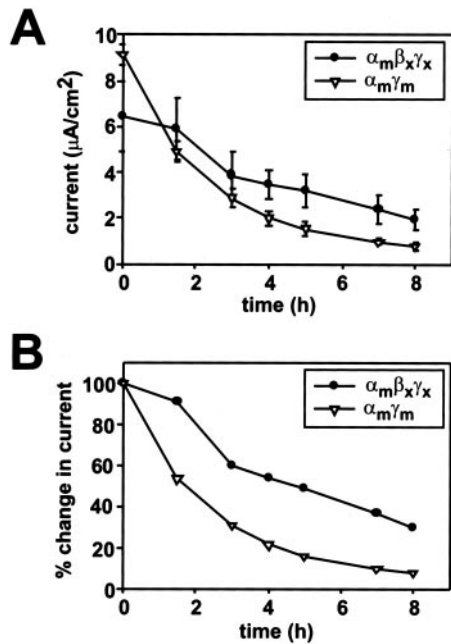


FIG. 5. Expression of β - and γ -xENaC with α -mENaC increases current stability upon CHX addition. MDCK I cells were infected with AVs encoding α - and γ -mENaC or α -mENaC plus β - and γ -xENaC. The following day, currents were monitored for 8 h after the addition of CHX. Raw data are plotted in A; the initial currents for each condition at the time of CHX addition were normalized to 100% and replotted in B.

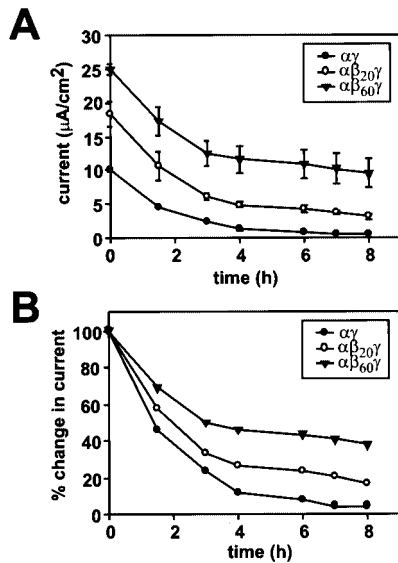


FIG. 6. Expression of β -mENaC correlates with residual current. MDCK cells were infected with AVs encoding α - and γ -mENaC (m.o.i. 60 each) and β -mENaC (m.o.i. 20 or 60). The decay in current was monitored for 8 h after the addition of CHX. Raw data are plotted in A; the initial currents for each condition at the time of CHX addition were normalized to 100% and replotted in B.

these studies, we have also exploited the DOX-dependent regulation of virally mediated ENaC expression to generate identically infected cells that express differing levels of ENaC.

Several studies have examined the biochemical stability of full-length ENaC subunits. However, given recent studies linking proteolytic cleavage with ENaC activity, quantitative changes in biochemical levels of ENaC subunits may not reflect changes in current. Moreover, we and others have observed noncoordinate changes in the levels of cell surface α -, β -, and γ -ENaC in response to some physiologic stimuli (6, 9, 20). It is

clear that individual ENaC subunits as well as combinations of subunits can traffic to the plasma membrane; however, the contribution of these subunits to ENaC activity is unclear. In combination, these complications make it difficult to simply correlate biochemical changes in ENaC subunit levels with alterations in current.

Whereas we readily detected full-length mENaC subunits in AV-infected MDCK cells, we did not observe significant levels of cleaved α - or γ -mENaC, even when all three subunits were expressed. Anti-V5 antibody detected two major bands that migrated close to the 97-kDa molecular mass standard in cells expressing only α -mENaC, similar to the pattern observed previously (13). A minor, faster migrating band was also detected that is larger than the reported 65-kDa furin-cleaved fragment of the α subunit (13, 14). When γ -mENaC was immunoprecipitated from AV-infected MDCK I cells, we observed a major band of \sim 93 kDa, with a minor form migrating at \sim 75 kDa, consistent with that of furin-cleaved γ -mENaC (13, 14). However, this band was observed even when γ -mENaC was expressed in the absence of the other two ENaC subunits, whereas furin-mediated cleavage of α - and γ -ENaC occurs only when all three subunits are co-expressed (13, 14). Whereas previous studies have used Western blotting to detect cleavage products of mENaC subunits that were doubly tagged at the amino and carboxyl termini, here we examined the expression of mENaC by immunoprecipitation of radiolabeled cells. It is important to note, however, that this method is biased toward detection of newly synthesized proteins and thus will underrepresent processed and cleaved forms in comparison with the steady state population of subunits that is detected by Western blot.

A universally accepted feature of ENaC subunit synthesis and assembly is the relatively short half-life of the total cellular pool of ENaC (9). A large fraction of newly synthesized ENaC is rapidly degraded ($t_{1/2} = 1$ –3 h), and a relatively small percentage reaches the plasma membrane (<1–20%) (2, 6, 9). Thus, changes in biochemical levels of full-length subunits probably reflect primarily the degradation of unassembled ENaC subunits in the endoplasmic reticulum. However, a wide range of half-lives (from \sim 15 min to $>$ 24 h) have been reported for ENaC subunits that reach the plasma membrane (4–6, 8, 9). Interestingly, in one recent study, biphasic decay of γ -xENaC in A6 cells upon the addition of CHX was noted, with \sim 80% of the full-length protein degraded within 1 h and a residual pool that remained stable for up to 12 h (21). Importantly, all of these studies quantitated the decrease with time of full-length subunits as opposed to cleavage products.

The difference in the current decay profiles between $\alpha\gamma$ - versus $\alpha\beta\gamma$ -mENaC-expressing cells that we observed was independent of the starting current and does not appear to be due to assembly of α - and γ -mENaC with canine β -ENaC. Whereas we detected canine β -ENaC message, no β -ENaC subunits could be detected in MDCK I cells, even upon expression of α - and γ -mENaC. Moreover, the biphasic current decay profile observed upon coexpression of α -mENaC with β - and γ -xENaC was similar to that in $\alpha\beta\gamma$ -mENaC-expressing cells, suggesting that the residual current component is not mENaC-specific. However, we cannot formally rule out the possibility that $\alpha\gamma$ -mENaC assembly with endogenous canine β -ENaC results in the formation of a channel with altered cell surface trafficking and turnover kinetics compared with mENaC holochannels.

We previously demonstrated that individual ENaC subunits biotinylated at the apical membrane of A6 cells are degraded with different kinetics (6). Moreover, we and others have observed changes in specific subpopulations of subunits in response to hormonal regulation of transport, both in whole cells

and at the apical membrane (6, 9, 20, 21). These observations are inconsistent with the idea that cell surface ENaC subunits in these cells are assembled exclusively into $\alpha\beta\gamma$ holochannels whose trafficking and turnover occurs in a congruent manner. We have used the term noncoordinate regulation to reflect this differential turnover of ENaC subunits and have proposed two models to explain our results (6, 9). In the first model, multiple stoichiometries of ENaC channels may exist at the cell surface, each with different turnover rates, such that the turnover of a single subunit would reflect its distribution among different types of channels. The second model proposes that channels may be remodeled at some post-endoplasmic reticulum site via selective trafficking of individual subunits. To begin to explore these possibilities, we have examined the expression and turnover of channels of varying stoichiometries. The data presented here are generally consistent with the first model. One possibility is that the rapidly decaying component of current in $\alpha\beta\gamma$ -expressing cells represents a pool of $\alpha\gamma$ channels, whereas the stable component represents $\alpha\beta\gamma$ channels. In support of this idea, we found a correlation between the fraction of initial current that remained stable upon CHX treatment and the amount of β -mENaC AV used to infect the cells. However, our data do not rule out the possibility that there also exists a pool of rapidly turning over $\alpha\beta\gamma$ channels. In this case, $\alpha\gamma$ channels retrieved from the membrane would be rapidly degraded, whereas $\alpha\beta\gamma$ channels would be differentially sorted, with some fraction degraded and the remainder able to recycle to the apical membrane. Interestingly, a recent study demonstrated that overexpression of β -ENaC but not α - or γ -ENaC in mouse airways resulted in increased sodium reabsorption, a finding that is consistent with the slower overall turnover of ENaC we observed in cells expressing all three subunits (22). Moreover, in another study, biphasic current decay was observed, although not noted, upon CHX addition to mouse cortical collecting duct cells that overexpressed β -ENaC (23). These observations suggest the possibility that changes in ENaC stoichiometry could affect ENaC channel stability *in vivo*.

The rapid initial decay that we observed for both $\alpha\gamma$ - and $\alpha\beta\gamma$ -expressing cells is consistent with some biochemical studies that measured short half-lives for cell surface ENaC subunits (4, 5). It is also possible that this population of channels is recognized as aberrant in some way and targeted for rapid degradation. For example, a recent elegant study demonstrates that mutant cystic fibrosis transmembrane conductance regulator that escapes the initial quality control machinery in the endoplasmic reticulum is still recognized as misfolded after reaching the plasma membrane and is degraded more rapidly than the wild-type protein (24). Conversely, the residual CHX-resistant pool of ENaC in $\alpha\beta\gamma$ -expressing cells may be selectively stabilized at the cell surface or may efficiently recycle to the plasma membrane after internalization. A region of ENaC has been found to interact with α -spectrin and could potentially tether the channels to the underlying cytoskeleton (25, 26); however, the functional significance of this interaction, particularly in polarized cells, is not clear. In addition, a fraction of ENaC has been demonstrated to localize in lipid rafts in A6 cells, although this was not observed for ENaC expressed in

MDCK cells (4, 27). ENaC association with lipid rafts could facilitate channel recycling, since rafts are significantly enriched in recycling endosomes relative to later compartments along the endocytic pathway (28). Finally, post-translational modification of ENaC (*e.g.* by carboxymethylation, by phosphorylation, or by cleavage at alternative sites) (16, 29) could regulate the stability or trafficking of $\alpha\beta\gamma$ -mENaC channels.

Acknowledgments—We thank Dr. Douglas Eaton for clones expressing β - and γ -xENaC, Dr. Mark Knepper for anti-ENaC antibodies, Dr. Rebecca Hughey for many helpful discussions and comments on the manuscript, and Dr. Robert Bridges for assistance with the kinetic analysis of ENaC current decay curves.

REFERENCES

- Rossier, B. C., Pradervand, S., Schild, L., and Hummler, E. (2002) *Annu. Rev. Physiol.* **64**, 877–897
- Valentijn, J. A., Fyfe, G. K., and Canessa, C. M. (1998) *J. Biol. Chem.* **273**, 30344–30351
- May, A., Puoti, A., Gaeggeler, H.-P., Horisberger, J.-D., and Rossier, B. C. (1997) *J. Am. Soc. Nephrol.* **8**, 1813–1822
- Hanwell, D., Ishikawa, T., Saleki, R., and Rotin, D. (2002) *J. Biol. Chem.* **277**, 9772–9779
- Alvarez de la Rosa, D., Li, H., and Canessa, C. M. (2002) *J. Gen. Physiol.* **119**, 427–442
- Weisz, O. A., Wang, J.-M., Edinger, R. S., and Johnson, J. P. (2000) *J. Biol. Chem.* **275**, 39886–39893
- Staub, O., Gautschi, I., Ishikawa, T., Breitschopf, K., Ciechanover, A., Schild, L., and Rotin, D. (1997) *EMBO J.* **16**, 6325–6336
- Kleyman, T. R., Zuckerman, J. B., Middleton, P., McNulty, K. A., Hu, B., Su, X., An, B., Eaton, D. C., and Smith, P. R. (2001) *Am. J. Physiol.* **281**, F213–F221
- Weisz, O. A., and Johnson, J. P. (2003) *Am. J. Physiol.* **285**, F833–F842
- Vallet, V., Chraïbi, A., Gaeggeler, H. P., Horisberger, J. D., and Rossier, B. C. (1997) *Nature* **389**, 607–610
- Adachi, M., Kitamura, K., Miyoshi, T., Narikiyo, T., Iwashita, K., Shiraishi, N., Nonoguchi, H., and Tomita, K. (2001) *J. Am. Soc. Nephrol.* **12**, 1114–1121
- Caldwell, R. A., Boucher, R. C., and Stutts, M. J. (2004) *Am. J. Physiol.* **286**, C190–C194
- Hughey, R. P., Mueller, G. M., Bruns, J. B., Kinlough, C. L., Poland, P. A., Harkleroad, K. L., Carattino, M. D., and Kleyman, T. R. (2003) *J. Biol. Chem.* **278**, 37073–37082
- Hughey, R. P., Bruns, J. B., Kinlough, C. L., Harkleroad, K. L., Tong, Q., Carattino, M. D., Johnson, J. P., Stockand, J. D., and Kleyman, T. R. (2004) *J. Biol. Chem.* **279**, 18111–18114
- Hardy, S., Kitamura, M., Harris-Stansil, T., Dai, Y., and Phipps, M. L. (1997) *J. Virol.* **71**, 1842–1849
- Rokaw, M. D., Wang, J.-M., Edinger, R. S., Weisz, O. A., Hui, D., Middleton, P., Shlyonsky, V., Berdiev, B. K., Ismailov, I. I., Eaton, D. C., Benos, D. J., and Johnson, J. P. (1998) *J. Biol. Chem.* **273**, 28746–28751
- Masilamani, S., Kim, G.-H., Mitchell, C., Wade, J. B., and Knepper, M. A. (1999) *J. Clin. Inv.* **104**, R19–R23
- McDonald, F. J., Price, M. P., Snyder, P. M., and Welsh, M. J. (1995) *Am. J. Physiol.* **268**, C1157–C1163
- Morris, R. G., and Schafer, J. A. (2002) *J. Gen. Physiol.* **120**, 71–85
- Planès, C., Blot-Chabaud, M., Matthay, M. A., Couette, S., Uchida, T., and Clerici, C. (2002) *J. Biol. Chem.* **277**, 47318–47324
- Booth, R. E., and Stockand, J. D. (2003) *Am. J. Physiol.* **284**, F938–F947
- Mall, M., Grubb, B. R., Harkema, J. R., O'Neal, W. K., and Boucher, R. C. (2004) *Nat. Med.* **10**, 487–493
- Auberson, M., Hoffmann-Pochon, N., Vandewalle, A., Kellenberger, S., and Schild, L. (2003) *Am. J. Physiol.* **285**, F459–F471
- Sharma, M., Pampinella, F., Nemes, C., Benharouga, M., So, J., Du, K., Bache, K. G., Papsin, B., Zerangue, N., Stenmark, H., and Lukacs, G. L. (2004) *J. Cell Biol.* **164**, 923–933
- Rotin, D., Bar-Sagi, D., O'Brodivich, H., Merilainen, J., Lehto, V. P., Canessa, C. M., Rossier, B. C., and Downey, G. P. (1994) *EMBO J.* **13**, 4440–4450
- Zuckerman, J. B., Chen, X., Jacobs, J. D., Hu, B., Kleyman, T. R., and Smith, P. R. (1999) *J. Biol. Chem.* **274**, 23286–23295
- Hill, W. G., An, B., and Johnson, J. P. (2002) *J. Biol. Chem.* **277**, 33541–33544
- Hao, M., Mukherjee, S., Sun, Y., and Maxfield, F. R. (2004) *J. Biol. Chem.* **279**, 14171–14178
- Shimkets, R. A., Lifton, R., and Canessa, C. M. (1998) *Proc. Natl. Acad. Sci. U. S. A.* **95**, 3301–3305